Published in final edited form as:
IEEE Trans Biomed Eng. 2008 June ; 55(6): 1744–1753.

An *In Vitro* Model of a Retinal Prosthesis

Ashish K. Ahuja,
Department of Electrical Engineering, University of Southern California, Los Angeles, CA 90089-2654 USA. He is now with Second Sight Medical Products, Sylmar, CA 91342 USA (aahuja@ 2-sight.com)

Matthew R. Behrend,
Department of Electrical Engineering, University of Southern California, Los Angeles, CA 90089-2654 USA (behrend@usc.edu)

Masako Kuroda,
Graduate School of Medicine, Kyoto University, Kyoto 611-0011, Japan (kuroda-m@mrf.biglobe.ne.jp)

Mark S. Humayun, and
Doheny Eye Institute, Keck School of Medicine, University of Southern California, Los Angeles, CA 90033-1035 USA (humayun@usc.edu)

James D. Weiland[*] **[Member, IEEE]**
Doheny Eye Institute, Keck School of Medicine, University of Southern California, Los Angeles, CA 90033-1035 USA

Abstract

Epiretinal prostheses are being developed to bypass a degenerated photoreceptor layer and excite surviving ganglion and inner retinal cells. We used custom microfabricated multielectrode arrays with 200-μm-diameter stimulating electrodes and 10-μm-diameter recording electrodes to stimulate and record neural responses in isolated tiger salamander retina. Pharmacological agents were used to isolate direct excitation of ganglion cells from excitation of other inner retinal cells. Strength-duration data *suggest* that, if amplitude will be used for the coding of brightness or gray level in retinal prostheses, shorter pulses (200 μs) will allow for a smaller region in the area of the electrode to be excited over a larger dynamic range compared with longer pulses (1 ms). Both electrophysiological results and electrostatic finite-element modeling show that electrode-electrode interactions can lead to increased thresholds for sites half way between simultaneously stimulated electrodes (29.4 ± 6.6 nC) compared with monopolar stimulation (13.3 ± 1.7 nC, $p <$ 0.02). Presynaptic stimulation of the same gan-glion cell with both 200- and 10-μm-diameter electrodes yielded threshold charge densities of 12 ± 6 and 7.66 1.30 nC/cm^2, respectively, while the required charge was 12.5 ± 6.2 and 19 ± 3.3 nC.

Keywords

Microelectrodes arrays; retinal electrophysiology; retinal prosthesis

[*](jweiland@doheny.org). .

Digital Object Identifier 10.1109/TBME.2008.919126

I. INTRODUCTION

BASED on the 2000 U.S. census, it is estimated that age-related macular degeneration (AMD) affects 1.75 million people over 40, and that by the year 2020, this population will grow to 3 million people [1], [2]. Retinitis pigmentosa (RP) is a genetic neurodegenerative disease that affects 1/4000 people worldwide [3]. Taken together, these diseases are the leading causes of retinal blindness. While there is significant degeneration of the outer retina and anatomical remodeling of the remnant inner retina [4], postmortem anatomical studies of patients with RP [5], [6] and AMD [7] have found that some inner retinal cells (78.4%) and ganglion cells (29.7%) can survive. This has led many research groups to investigate extracellular electrical stimulation as a means of restoring visual function to patients by implanting an epiretinal [8] or subretinal [9]-[11] microelectrode array. Early chronic implants have allowed subjects to detect motion and changes in ambient light, and discern simple shapes [12], [13].

Current active implants stimulate groups of cells nonspecifically because of electrode size (50-500 μm diameter) [14]. Although it may be advantageous to address ganglion cells individually with smaller electrodes due to the specific function of various ganglion cell classes that tile the retina and to afford a higher resolution implant, small electrodes may not be realizable in devices that might be available in the near future due to technical limits such as charge density safety limits (i.e., O_2 and H_2 evolution, metal dissolution, and local pH shifts) and tissue heating considerations [15], [16], as well as challenges associated with the routing of many leads per unit area [17]. Thus, the next generation of retinal prostheses will operate by stimulating groups of cells with large electrodes. Investigating the physiological basis of electrically stimulated retina using microfabricated multielectrode arrays (MEAs) with large stimulating discs may allow us to understand the origin of elicited percepts and improve the level of vision achievable by optimizing stimulus parameters.

The electrophysiological response of the retina to electrical stimulation has been studied extensively using an isolated vertebrate retina model. Many investigations employed single metal wire or conical shaped electrodes for extracellular stimulation and recording [18]-[23]. Others used these electrodes for stimulation but recorded excitatory and inhibitory current into ganglion cells using a whole cell patch clamp technique [24], [25]. Multielectrode array stimulating and recording that most accurately mimics the electrode-tissue interface in a retinal prosthesis has also been investigated using stimulating electrodes that varied in diameter over a large range (6-1500 μm) [26]-[30]. These studies primarily investigated charge density thresholds for various sized electrodes, and the relative threshold for somatic excitation compared with axonal stimulation.

This study used custom microfabricated MEAs that facilitated several novel experiments that closely approximate epiretinal prosthesis operation. The MEAs were designed with stimulating electrodes mimicking the size and spacing of implantable devices that might be available in the near future (200 μm diameter, 500 μm center-to-center spacing), and recording electrodes capable of recording single-unit responses from a ganglion cell. MEAs with a similar recording electrode pitch have been used to record from a good fraction of ganglion cells in tiger salamander the animal model used here [31]. This custom array allowed us to study the spatial spread of ganglion cell activation and its dependence on pulse duration and amplitude. Because the spacing of stimulating and recording electrodes was precisely controlled during MEA fabrication, we could record the retinal ganglion cell (RGC) response between adjacent, simultaneously activated electrodes. The conductive media electrostatics module within FEMLAB finite-element modeling software (COM-SOL, Los Angeles, CA) was used to further investigate the electrode-electrode interaction. Pharmacological agents were used to study the frequency dependence of direct stimulation

of ganglion cells and stimulation of presynaptic cells (e.g., bipolar and amacrine cells). Stimulation with both large and small electrodes was done to assess how threshold charge depends on electrode size.

II. METHODS

A. Tissue Preparation

All animal protocols were approved by the Institutional Animal Care and Use Committee at the University of Southern California. Data were collected from 22 larval tiger salamander retinas (*Ambystoma tigrinum*) using established methods [32]. Tiger salamanders were kept at 5 [1]C in a 12 h light/dark cycle. Salamanders were rapidly decapitated and pithed in dim room light. Eyes were enucleated and eyecups were placed in bicarbonate solution (in millimeters): 110 NaCl, 2 KCl, 30 $NaHCO_3$, 1.5 $CaCl_2$, 1.6 $MgCl_2$, 10 glucose, 0.01 ethylenediaminetetraacetic acid (EDTA) that is bubbled with 5% CO_2/95% O_2. One millimeter square pieces of retina were cut and placed on a custom made plunger (used to keep the retina in place on the array) outfitted with a microporous dialysis membrane (used to allow the exchange of nutrients between the tissue and the perfusate) (spectrum molecularporous membrane (molecular weight cutoff 12 000-14 000), Spectrum Laboratories, Inc., California). The plunger was then inserted into a cylindrical mount, which was attached to the MEA with an adhesive silicone elastomer; the RGC side of the tissue was gently pressed onto the array while being observed through an inverted microscope. The retina was perfused at 3-5 ml/min with oxygenated bicarbonate solution.

B. Custom Multielectrode Arrays

Custom multielectrode arrays were designed with four 200-μm-diameter stimulating electrodes (500 μm center-to-center spacing), and fifty-six, 10-μm-diameter recording electrodes arranged with radial symmetry with respect to the stimulating electrode edge (i.e., at distances of 50, 100, and 150 μm from the stimulating electrode edge). The average center-to-center spacing of recording electrodes was approximately equal to the spacing employed in arrays used to sample every ganglion cell in a given retinal patch in the tiger salamander [33]. Photomasks were laid out using Tanner L-Edit CAD software (Tanner Research, Pasadena, CA).

MEAs were fabricated at the Keck Center for Photonics at the University of Southern California. Details of the two photomask photolithographic process flow for fabrication of MEAs with Pt leads and silicon nitride/SU-8 insulation are described elsewhere [34], [35].

To minimize electrochemical impedance and maximize area, 200-μm-diameter stimulating electrodes were electroplated using an ammonium hexachloroplatinate bath [17 mM $(NH_4)_2PtCl_6$ + 250 mM Na_2HPO_4], a Princeton 2263 potentiostat, and a custom three-electrode electrochemical cell [36]. The cell allowed for proximal placement of an Ag/AgCl reference electrode and large Pt wire mesh counter electrode next to the working electrode to be plated. Deposition was done using cyclic voltammetry (U = −0.8 to 0.6 V vs. Ag/AgCl, scan rate 200 mV/s for 180 cycles). Cyclic voltammetry allowed for a resetting of the diffusion layer in each scan so that a “mushroom” -shaped electrode profile was avoided, which is sometimes observed in static potential electroplating [37]. Here, the resulting film was geometrically well confined to the area defined by the photolithographic process flow, as shown in Fig. 1. Tenmicrometer-diameter stimulating electrodes consisted of thinfilm e-beam evaporated Pt. These electrodes were not electroplated with ammonium hexachloroplatinate since they were also used as recording electrodes, and such low impedance electrodes typically recorded field potentials and not single unit activity.

C. Electrical Stimulation and Recording

Biphasic cathodic-first current pulses were generated using a stimulus generator (STG 2001, Multichannel Systems, Reutlingen, Germany). Up to two electrodes could be selected as stimulating electrodes and the stimuli programmed independently for each electrode. Any of the 60 MEA electrodes, either large or small, could be selected for stimulation. A platinum wire placed in the perfusate solution in the MEA chamber served as the ground electrode for all stimulus protocols. RGC responses were amplified by 1100 using an MEA 1060 preamplification board (Multichannel Systems, Reutlingen, Germany). Definition of stimulus pulse parameters and data collection was done using software from MultiChannel Systems (MC Stimulus 2.0.6.0, MC Rack 3.4.0). Data were sampled at 20 kHz; action potentials were recorded with a 300-3000 Hz bandpass filter. Symmetric biphasic cathodic-first stimulus pulses varied in amplitude from 1 to 500 μA, and time per phase varied from 20 μs to 1 ms. An oscilloscope was used to monitor current output of the stimulating electrode to ensure that the specified pulse was delivered and not cutoff due to stimulus amplifier compliance voltage limits. Recorded spikes had a similar waveform shape and duration as those reported by others recording from ganglion cell somas in tiger salamander [31].

D. Experimental Protocol

After the retina was placed RGC side down on the array, a 40 ms full-field light flash (4×10^3 cd/m^2) was given to determine which electrodes were well coupled to cells. This information also assured that adjacent electrodes were recording from different cells. Only electrodes showing an SNR >5:1 were studied to facilitate data processing. All electrical stimulation protocols used trains of 50 biphasic pulses. A stimulus value was deemed above threshold if it elicited a response over 75% of the time (i.e., ≥38 spikes elicited in a 50 pulse train). With the exception of stimulus frequency studies, the pulse repetition rate was 2.5 Hz. With the exception of strength duration studies, all pulses were 400 μs per phase, cathodic-first biphasic pulses with no interphase delay.

E. Pharmacological Agents and Artifact Subtraction

Pharmacological agents were used for the purposes of isolating the source of the neural response (i.e., presynatically driven responses vs. direct excitation of RGCs) by mixing with the perfusate. A cocktail of 6-cyano-7-nitroquinoxaline [CNQX; competitive !-amino-3-hydroxy-5-methylisoxazole-4-propionic acid (AMPA)/kainite receptor antagonist, 75 μM], 2-amino-5-phosphonovaleric acid [APV; competitive *N*-methyl D-aspartate (NMDA) receptor antagonist, 400 μM], and *cis*-2,3-piperidine dicarboxylic acid [PDA; agonist to NMDA receptor (NMDAR), 1 mM] were used in nine experiments to block NMDA and non-NMDA-mediated glutamatergic synaptic input to RGCs [26], [27]. In five separate experiments, $CdCl_2$ (Ca^+ channel blocker, 1 mM) was also used to abolish synaptic transmission. Both methods abolished light responses entirely. These manipulations allowed for the direct stimulation of ganglion cells to be separated from longer latency stimulation of presynaptic cells. Because direct stimulation has a latency <7 ms, responses of this type were contaminated by the stimulus artifact. A method of artifact subtraction has been described by others and is used here (Fig. 2) [25], [27]. An artifact for a pulse that does not evoke a response can be subtracted from an artifact with a superimposed response to reveal the elicited spike. Tetrodotoxin (TTX, Na^+ channel blocker) was also employed for the purposes of artifact subtraction as described in the referenced works. Another method used for detecting a spike hidden in the stimulus artifact was used in the case where neighboring electrodes were equidistant from the stimulation site, and the resulting recorded artifact amplitude was therefore similar. In such a case, a spike could be visualized as a difference in the two artifact waveforms (Fig. 7).

F. Finite-Element Modeling of Electrode-Electrode Interaction

Finite-element model (FEM) simulations were designed with FEMLAB software (Comsol Inc., Los Angeles, CA). The simulations utilized the conductive media electrostatics module within FEMLAB. Tetrahedral elements were used to define the model meshes. Microelectrodes were modeled as 200-μm-diameter circular discs (500 μm center-to-center spacing), flush with the surrounding dielectric of the array substrate, and centered beneath the base of a larger hemispherical volume of saline medium. The radius of the medium surrounding the electrode was large enough to approximate an infinite volume. The hemispherical surface defining the upper boundary served as the ground electrode (zero-potential boundary). Microelectrode conductivity was 5×10^7 S/m (an isopotential surface) and hemispherical medium conductivity was 1.54 S/m [38]. This model represents two adjacent flat microelectrode discs immersed in saline solution. A fixed current of 30 μA was injected into the lower boundary surface of the microelectrodes.

G. Data Analysis

The RGC response data were converted to Amsterdam Subversive Center for Information Interchange (ASCII) format using MC_DataTool V 2.1, and poststimulus time histograms (PSTHs) were generated using custom written MATLAB code. The code performed artifact subtraction and detected spikes with a simple threshold test. All variance measurements (i.e., ±) represent standard deviations. Standard deviations, best fit curves, and Student's *t*-tests were calculated using EXCEL and Igor Pro V 5.03 software. All plots were also generated using Igor Pro.

III. RESULTS

A. Response Latency

Spikes were elicited by both the direct excitation of ganglion cells and the excitation of inner and outer retinal cells and their subsequent synaptic excitation of ganglion cells. The former had latencies of 0.5-7 ms with respect to the onset of the stimulus pulse while the later had latencies of 3-400 ms. The source of excitation was ascertained using both the CNQX/APV/PDA cocktail and $CdCl_2$ (described in Section II). Both of these methods have been employed by others to determine the mechanism of spike generation [24], [25], [27], [39]. Engaging inner retinal cells sometimes resulted in reverberating activity that could last up to 400 ms (Fig. 3).

B. Excitation Radius Versus Stimulus Amplitude

Presynaptic excitation of ganglion cells further from the stimulating site had a higher threshold for stimulation compared with presynaptic excitation of cells closer to the stimulating electrode when using 400 μs per phase pulses. Cells 50 μm from the electrode edge had a threshold current of 27.75 ± 8.66 μA compared with cells 433 μm away that had a threshold of 68 ± 23.09 μA ($p < 0.01$; $n = 42$ cells, and $R^2 = 0.58$; Fig. 4). Cell location was taken as the center of the recording electrode used.

Strength duration data for cells 100, 150, and 235 μm away from the stimulating electrode edge ($n = 9$ total cells) were collected for 60, 100, 200, 400, 600, 800, and 1000 μs biphasic pulses (one cell was able to be excited with a 20 μs pulse; in other instances, the minimum pulse duration was set by the maximum amplitude that could be achieved without saturating the preamplifiers) (Fig. 5).

Two parameters of interest for strength duration curves are the rheobase and the chronaxie [40]. The rheobase is the minimum current required to stimulate a cell regardless of duration. The chronaxie is the pulse duration for which the threshold current is twice the

rheobase current. Power curve fitting ($y = y_o + Ax^p$) was done in Igor Pro software to determine chronaxie and rheobase values, where the rheobase was defined by the y-axis offset (y_o) of the curve fit. Average rheobase values were 6.5 ± 0.7, 27.8 ± 16.0, and 46.2 ± 53.5 μA, and average chronaxie values $\left(\sqrt[p]{y_0/A}\right)$ were 179 ± 7.1, 481 ± 95.0, and 600 ± 77.8 μs for cells 100, 150, and 235 μm away fromthe stimulating electrode edge, respectively.

C. Monopolar, Dual Monopolar, and Bipolar Stimulation

For experiments in which a cell was well coupled to a recording electrode in between and equidistant from adjacent 200 μm stimulating electrodes, the relative charge thresholds for monopolar, dual monopolar (i.e., adjacent electrodes driven equally and simultaneously), and bipolar stimulation were compared.

Monopolar stimulation required an average charge threshold of 13.3 ± 1.7 nC, compared with 29.4 ± 6.6 nC for dual monopolar stimulation, and 10.0 ± 3.4 nC for bipolar stimulation ($p < 0.02$ in comparing the statistical difference of all three data sets with each other; $n = 5$ cells for each condition). The fact that stimulating two adjacent electrodes simultaneously with the same polarity increased the charge threshold by approximately 212% was consistent with FEM of electrostatic interactions between electrodes. Fig. 6 shows simulation results from two 200-μm-diameter Pt electrodes stimulated in monopolar, dual monopolar, and bipolar configurations.

The relationship between the membrane voltage (V_m) and external uniform electric field (E) for a passive nonconducting spherical cell is $V_m = -(3/2)Er\cos\theta$, where r is the cell radius and θ is the angle of the field with respect to the direction normal to the cell membrane [41]. A threshold voltage must be induced across the membrane to trigger voltage-gated ion channels, and hence, the local field vector is a critical parameter in excitation. The finite-element model predicts a “dead region” at the midpoint between stimulation sites for the dual monopolar configuration due to the field of one electrode perturbing the field of the other, which increases the threshold relative to monopolar stimulation in this location.

D. Frequency Dependence of Presynaptic and Direct Ganglion Cell Excitation

As the frequency of stimulation is increased, the response rate of all presynapitcally driven responses approaches zero ($n = 6$ cells) at 10 Hz ± 4.67 Hz, while direct ganglion cell stimulation persists up to 500 Hz ($n = 3$ cells; Fig. 7). Four hundred microseconds per phase pulses were delivered at pulse repetition rates ranging from 2.5 to 500 Hz. Both a CNQX/APV/PDA cocktail and the calcium channel blocker $CdCl_2$ (1 mM) were used in separate experiments to distinguish the frequency limits of excitation of ganglion cells and cells presynaptic to the ganglion cell layer.

E. Charge and Charge Density Thresholds Using 200- and 10-μm-Diameter Electrodes

Presynaptic excitation of the same ganglion cell ($n = 5$ cells) with both 200- and 10-μm-diameter electrodes with 400 μs pulses yielded threshold charge densities of 12 ± 6 nC/cm^2 (average cell–electrode edge distance of 87.5 μm) and 7.66 ± 1.30 mC/cm^2 (average cell–electrode edge distance of 68.8 μm), respectively. The average charge required, however, was 12.5 ± 6.2 nC for the 200-μm-diameter electrode and 19 ± 3.3 nC for the 10-μm-diameter electrode, suggesting that a threshold amount of charge, not charge density, must be injected into the extracellular space to elicit a presynaptically driven response.

IV. DISCUSSION

Both short (0.5–7 ms) and long (3–400 ms) latency spikes have been observed; the former due to the direct excitation of ganglion cells and the latter due to the excitation of inner retinal cells presynaptic to the RGC layer. These latencies are in good agreement with other studies [19], [25], [27]. Ganglion cells can exhibit both phasic (single spike output) and tonic (multiple spike output) behavior [42], and while both types of responses were observed with regard to direct ganglion cell stimulation, unless stated otherwise, all the data presented are with regard to presynaptic excitation.

Reverberating activity lasting 100 ms has been reported in the stimulation of rabbit retina with conical shaped electrodes [25] and wire electrodes [43], and with transcorneal stimulation in cat retina using concentric bipolar electrodes [44]. Using 200 μm stimulating electrodes, we observed similar activity lasting as long as 400 ms. Fried's study has suggested that this activity is due to the excitation of both bipolar cells, which release the excitatory transmitter glutamate and amacrine cells, which provide feedforward inhibition to ganglion cells and feedback inhibition to bipolar cells. The longer lasting reverberating response observed in this study may be due to the fact that much larger stimulating electrodes were used. These electrodes have an excitation field that permeates deeper into the retina than smaller, conical electrodes, engaging a larger area of the inner retina. It is interesting to note that reverberating activity can be observed without the excitation of ganglion cells directly (i.e., short latency response). This was also observed by Crapper and Noell using pulses of a similar duration (0.5 ms) [43]. This may be due to the fact that graded potential cells are reported as having longer chronaxies [30]. Greenberg used >1 ms pulses to target bipolar cells while Fried *et al.* used pulses <0.15 ms to target ganglion cells directly. Here, we are between the two sets of pulse durations in time. Studies in a retinal degenerate animal will be required to see if this reverberation is curtailed due to anatomical remodeling [4] and changes in the physiological response of cells [45].

Our results agree with earlier investigations of threshold versus distance. Ziv *et al.* investigated the target cell location using threshold data from the stimulation of RGCs in rabbit to build a mathematical model of the excitation field around a conical-tipped electrode [46]. It was reported that threshold had a $1/r^{0.84}$–$1/r^{3.19}$ dependence on distance from the stimulation tip, in slight contrast with the strict $1/r^2$ dependence predicted by Coulomb's law. We report a $1/r^{1.69}$ dependence based on threshold amplitude versus distance from the stimulating edge data (Fig. 4) using 200-μm-diameter Pt electrodes. This size electrode does not allow it to be treated as a point source; however, the relationship is in good agreement with the investigation using conical tipped electrodes. While comparisons of this relationship to Coulomb's law are relevant, it is important to keep in mind that, since the data represent presynaptic excitation, the field profile will be perturbed by the retinal tissue, which is anisotropic. Moreover, the data are not a direct measure of the field strength as described by Coulomb's law, but rather the electrical response of many retinal cells converging on the ganglion cell being recorded from.

The strength duration data suggest a strategy for coding brightness. If amplitude will be used for the coding of brightness or gray-level in retinal implants, using shorter pulses may allow for a smaller region in the area of the electrode to be excited over a larger dynamic range. For example, for a 1 ms pulse, the threshold current required to stimulate a cell 150 μm away (27 μA) is 4.75 times greater than that required to stimulate a cell 100 μm away (6 μA). Comparatively, for a 200 μs pulse, the threshold current required stimulate a cell 150 μm away (136 μA) is 10.5 times greater than that required to stimulate a cell 100 μm away (13 μA). This trend is also reflected in the chronaxies of the strength duration curves at various distances from the stimulating electrode: cells proximal to the stimulating electrode

have lower chronaxies than cells further away. Shorter pulses may more effectively decouple amplitude-dependent parameters from excitation area. The underlying assumption in this hypothesis is that increased brightness of phosphenes in retinal implant subjects is at least partially due to individual ganglion cells responding differently to threshold and suprathreshold stimulation, and not solely due to more cells being excited. There is good evidence for this in the work of Crapper and Noelle, who showed that the number of bursts (or total ganglion cell spikes) increased with injected current, while the frequency of spiking within bursts remained constant [43].

A similar conclusion has been made in studies on peripheral nerve stimulation, where shorter pulses yielded improved selectivity between different fascicles in cat sciatic nerve [47]. In deep brain stimulation of the subthalamic nucleus in order to decrease contralateral wrist rigidity [required clinical effect (RCE)] in patients suffering from Parkinson's disease, it was found that shorter pulses most reliably result in the RCE without causing side effects (i.e., the stimulation of nearby fibres resulting in pain) compared with longer duration pulses [48].

There was greater variability in stimulus threshold for sites farther away from the stimulating electrode. The standard deviation for the stimulation of cells 433 μm away is 2.6 times greater than that for cells 50 μm away. This is also shown clearly in the log-log plots of the strength duration data (Fig. 5), where curves for cells 100 μm away are more closely correlated with each other than all cells greater than 100 μm away. Because the data presented in Fig. 5 involve the excitation of inner retinal cells, this variability may be due to the fact that a greater portion of the nonlinear retinal network is engaged at greater distances from the stimulating site, making the ganglion cell response more complex at these distances.

The difference in the suprathreshold PSTHs between monopolar and bipolar stimulation indicate that a ganglion cell's response is dependent on the stimulation source and sink. It is likely that, because multiple inner retinal cells converge on a single ganglion cell, the response of that ganglion cell is dependent on the different portions of this inner retinal network that are excited. As can be seen from the finite-element modeling results in Fig. 6, whereas the electric field is highly divergent in the area of the stimulating electrode itself in monopolar stimulation, in bipolar stimulation having a return electrode, which is in close proximity to the stimulating electrode, it also creates a significant spatial gradient that will likely penetrate the inner retina. Therefore, while the same ganglion cell is stimulated in both cases, the envelope of the PSTH is different in both cases. This suggests that, even with same target ganglion cell, current source and sink (i.e., monpolar vs. bipolar stimulation) can affect the output spike train, and perhaps, the elicited percept.

Electric field interaction leads to an area of decreased excitability in between two simultaneously active electrodes. Electrode-electrode interactions have also been observed in cochlear implant (CI) patients. In psychophysical tests conducted on these patients, it was found that stimulus schemes that allowed for only interleaved pulsing between adjacent electrodes resulted in improved scores in the closed-set identification of consonants and the open-set recognition of words and sentences when compared with schemes incorporating simultaneous pulsing between adjacent electrodes [49], [50]. These interactions then should be ignored when making assumptions about the overall field profile at the multielectrode array-retina interface. At the same time, the multielectrode array-retina spacing must be minimized in order to observe this effect. As can be seen in the finite-element results, at some distance, the z-components of these fields align such that no zone of inactivity should be observed. Vector summation in CI subjects in regions between electrodes has also been reported presumably due to an increased electrode-cochlea spacing compared with

electrode–retina spacing in this study [51]. Another retinal stimulation study employing multiple 10-μm-diameter electrodes with 60 μm center-to-center spacing has showed that each electrode can stimulate cells in the same manner (i.e., same targeted cell and response latency) whether all electrodes are driven individually or at the same time [27]. However, this case is very different from what has been studied here because of electrode size. The falloff of the excitation field into the tissue is dictated by electrode radius, and the large discs employed here will more readily engage a greater portion of the inner retina (e.g., bipolar and amacirne cells), whereas smaller 10 μm discs can more specifically target the ganglion cell layer. It is clear therefore that the effect of electrode-electrode interactions will be dependent on electrode size and pitch.

The retina relays visual information to higher cortical centers by varying spike timing. The maximum frequency at which certain classes of ganglion cells can generate spikes is approximately 260 Hz, and so it is important that cells can be electrically driven at this rate if we hope to truly mimic retinal function [52]. We have found that presynaptic excitation is suppressed at 10 ± 4.67 Hz, while ganglion cells can directly be excited up to 500 Hz. Our results for presynaptic excitation are in excellent agreement with the two other studies that investigated the frequency dependence of stimulation using conical electrodes (40 μm^2) and Pt electroplated microdiscs (6-25 μm diameter) [25], [27] that also report the suppression of presynaptic excitation of RGCs at ~10 Hz in both the rat and rabbit. We have, however, found an even higher maximum firing rate of RGCs compared with previous reports. The suppression of presynaptic excitation has been attributed to comparatively longer inhibitory input current from amacrine cells (≤100 ms) compared to the excitatory bipolar input. This value of 100 ms is in good agreement with a cutoff frequency of approximately 10 Hz. This result suggests that, although an epiretinal stimulating electrode can stimulate inner retinal cells giving rise to a longer latency response, there exists a wide frequency range in which RGCs are addressed without input from other cells. This would eliminate complex input due to the reported reverberating response.

Understanding the dependence of threshold charge and charge density on decreasing electrode size will be critical in designing higher resolution prostheses. A recent review has compiled the results of studies using different sized stimulating electrodes in retinal stimulation experiments in animals and in subjects [27]. While results in animals generally show that threshold charge decreases with electrode diameter, the threshold charge density increases. This suggests a complex relationship between thresholds and electrode size, possibly due to an inhomogeneous current distribution at the surface of the electrode that evolves during the time course of the stimulus pulse [53], [54]. The trend for thresholds required for eliciting phosphenes in human subjects is less clear. A study on the perceptual thresholds in three subjects implanted with an epiretinal device showed there was no significant difference in charge thresholds between 250- and 500-μm-diameter electrodes [14]. We observe a similar dependence on absolute charge when stimulating the same RGC with 10- and 200-μm-diameter electrodes with similar edge-to-edge spacing between stimulating and recording electrodes. This relative ratio of electrode sizes used in this study is the largest reported thus far, and represents sizes that will be used in near-term epiretinal implants to those that might be used to address individual cells. Because comparative thresholds were obtained from stimulating the same target cell using the same preparation and the same array, the tissue-array spacing was effectively held constant. While stimulation with large electrodes was approximately 30 times below established electrochemical safe-charge injection limits of 0.35 mC/cm^2 [16], stimulation with small electrodes was approximately 20 times greater than this limit.

This dependence on absolute charge is counterintuitive since it is the local voltage gradient that is induced across the cell membrane that stimulates the cell. This would suggest that

electrode current density should be the determining factor. Because the data presented here represent presynaptic excitation one reason however for a dependence on absolute charge is the following. The excitation field of a large electrode extends further into the retinal tissue (to stimulate bipolar, amacrine, and other deeper cells) than a small electrode with the same charge density. This is because the spatial voltage gradient in the vicinity of the electrode is dependent on size [55]. Hence, larger electrodes will require a lower threshold charge density than smaller ones regarding presynaptic stimulation. Further array studies with a large range of electrode sizes fabricated on the same substrate will provide deeper insight into the dependence of stimulation on charge and charge density, and combined with visual psychophysical testing in implanted subjects, should help deduce which retinal elements are excited in the eliciting of phosphenes.

Acknowledgments

The authors thank A. P. Sampath, H. Okawa, and M. C. Hauer.

This work was supported in part by the Research to Prevent Blindness under the National Science Foundation (NSF) Grant EEC-0310723 and in part by the W. M. Keck Foudation. The work of M. Behrend was supported in part by the Fannie and John Hertz Foundation and in part by the National Defense Science and Engineering Grant.

Biography

Ashish K. Ahuja received the B.S. degree in applied physics and the M.S. degree in electrical engineering from Columbia University, New York, in 1999 and 2002, respectively, and the Ph.D. degree in electrical engineering—electrophysics from the University of Southern California, Los Angeles, CA, in 2007.

He was with the Department of Condensed Matter Physics and also the Department of Fiber Optics Devices, Bell Laboratories, for two years. He is currently a Postdoctoral Fellow at Second Sight Medical Products, Sylmar, CA, where he has been engaged in the development of implantable retinal prosthesis for the blind. His current research interests include retinal implant fitting and psychophysics testing of retinal implant subjects.

Matthew R. Behrend received the B.S. degree in electrical engineering in 2004 from the University of Southern California, Los Angeles, CA, where he is currently working toward the Ph.D. degree from the electrical engineering - electrophysics department.

He was engaged in research on novel pulsed power electronics for real-time microscopy of pulsed cells. He was a summer hire at Teen Read Week (TRW) in 2001 and Northrop Grumman in 2003. His current research interests include the design of extremely high-resolution bioelectronic interfaces.

Masako Kuroda, photograph and biography not available at the time of publication.

Mark S. Humayun received the B.S. degree in biomedical engineering from Georgetown University Washington, DC, in 1984, the M.D. degree in ophthalmology from Duke University, Durham, NC, in 1989, and the Ph.D. degree in biomedical engineering from the University of North Carolina, Chapel Hill, in 1994.

He was a faculty member at Johns Hopkins University, Baltimore, MD, and in 2001, was promoted to Associate Professor. He is currently a Professor of Ophthalmology, Biomedical Engineering, and Cell and Neurobiology at the Doheny Eye Institute, Keck School of Medicine, University of Southern California, Los Angeles. He is the author or coauthor of more than 100 articles published in peer-reviewed journals, chapters, and holds more than 10 issued-patents. He is the Director of the National Science Foundation Biomimetic MicroElectronics Systems Engineering Research Center, and the Department of Energy Artificial Retina Project.

Dr. Huymayun was the recipient of the R&D Magazine Innovator of the Year Award in 2005.

James D. Weiland (S'92-M'97) received the B.S. degree in electrical engineering in 1988, the M.S. and Ph.D. degrees in biomedical engineering in 1993 and 1997, respectively, and the second M.S. degree in electrical engineering, in 1995, all from University of Michigan, Ann Arbor.

In 1997, he joined the Wilmer Ophthalmological Institute, Johns Hopkins University, as a Postdoctoral Fellow, and in 1999, became an Assistant Professor of Ophthalmology. During 2001, he was an Assistant Professor at the Doheny Eye Institute, University of Southern California, where he is currently an Associate Professor of Ophthalmology and Biomedical Engineering. His current research interests include retinal prostheses, neural prostheses, electrode technology, visual-evoked responses, and implantable electrical systems.

Dr. Weiland is a member of the IEEE Engineering in Medicine and Biology Society (EMBS), the Biomedical Engineering Society, the Sigma Xi, and the Association for Research in Vision and Ophthalmology.

REFERENCES

[1]. Friedman DS, O'Colmain BJ, Munoz B, Tomany SC, McCarty C, de Jong PT, Nemesure B, Mitchell P, Kempen J. Prevalence of age-related macular degeneration in the United States. Arch. Ophthalmol. 2004; 122:564–72. [PubMed: 15078675]

[2]. Klein R, Klein BE, Jensen SC, Meuer SM. The five-year incidence and progression of age-related maculopathy: The Beaver Dam eye study. Ophthalmology. 1997; 104:7–21. [PubMed: 9022098]

[3]. Berson EL. Retinitis pigmentosa the friedenwald lecture. Invest. Ophthalmol. Vis. Sci. 1993; 35:1659–1676. [PubMed: 8473105]

[4]. Marc RE. Neural remodeling in retinal degeneration. Prog. Retin. Eye Res. 2003; 22:607–655. [PubMed: 12892644]

[5]. Santos A, Humayun MS, de Juan E Jr. Greenburg RJ, Marsh MJ, Klock IB, Milam AH. Preservation of the inner retina in retinitis pigmentosa. A morphometric analysis. Arch. Ophthalmol. 1997; 115:511–515. [PubMed: 9109761]

[6]. Stone JL, Barlow WE, Humayun MS, de Juan E Jr. Milam AH. Morphometric analysis of macular photoreceptors and ganglion cells in retinas with retinitis pigmentosa. Arch. Ophthalmol. 1992; 110:1634–1639. [PubMed: 1444925]

[7]. Kim SY, Sadda S, Pearlman J, Humayun MS, de Juan E Jr. Melia BM, Green WR. Morphometric analysis of the macula in eyes with disciform age-related macular degeneration. Retina. 2002; 22:471–477. [PubMed: 12172115]

[8]. Humayun MS. Intraocular retinal prosthesis. Trans. Amer. Ophthal-mol. Soc. 2001; 99:271–300.

[9]. Chow AY, Peachey NS. The subretinal microphotodiode array retinal prosthesis. Ophthalmic Res. 1998; 30:195–198. [PubMed: 9618724]

[10]. Zrenner E, Miliczek KD, Gabel VP, Graf HG, Guenther E, Haemmerle H, Hoefflinger B, Kohler K, Nisch W, Schubert M, Stett A, Weiss S. The development of subretinal microphotodiodes for replacement of degenerated photoreceptors. Ophthalmic Res. 1997; 29:269–280. [PubMed: 9323718]

[11]. Rizzo JF III, Wyatt J, Loewenstein J, Kelly S, Shire D. Methods and perceptual thresholds for short-term electrical stimulation of human retina with microelectrode arrays. Invest. Ophthalmol. Vis. Sci. 2003; 44:5355–5361. [PubMed: 14638738]

[12]. Chow AY, Chow VY, Packo K, Pollack HJS, Peyman GA, Schuchard R. The artifical silicon retina microchip for the treatment of vision loss from retinits pigmentosa. Arch. Ophthalmol. 2004; 122:460–469. [PubMed: 15078662]

[13]. Humayun MS, Weiland JD, Fujii GY, Greenberg R, Williamson R, Little J, Mech B, Cimmarusti V, Van Boemel G, Dagnelie G, de Juan E. Visual perception in a blind subject with a chronic microelectronic retinal prosthesis. Vis. Res. 2003; 43:2573–2581. [PubMed: 13129543]

[14]. Mahadevappa M, Weiland JD, Yanai D, Fine I, Greenberg RJ, Humayun MS. Perceptual thresholds and electrode impedance in three retinal prosthesis subjects. IEEE Trans. Neural Syst. Rehabil. Eng. Jun; 2005 13(2):201–206. [PubMed: 16003900]

[15]. Brummer SB, Turner MJ. Electrochemical considerations for safe electrical stimulation of the nervous system with platinum electrodes. IEEE Trans. Biomed. Eng. Jan; 1977 24(1):59–63. [PubMed: 851475]

[16]. Brummer SB, McHardy J, Turner MJ. Electrical stimulation with Pt electrodes: Trace analysis for dissolved platinum and other dissolved electrochemical products. Brain Behav. Evol. 1977; 14:10–22. [PubMed: 13907]

[17]. Weiland JD, Humayun MS. A biomimetic retinal stimulating array. IEEE Eng. Med. Biol. Mag. Sep-Oct;2005 24(5):14–21. [PubMed: 16248113]

[18]. O'Hearn M, Sadda TSR, Weiland JD, Maia M, Margalit E, Humayun MS. Electrical stimulation in normal and retinal degeneration (RD1) isolated mouse retina. Vis. Res. 2006

[19]. Jensen RJ, Rizzo JF III, Ziv OR, Grumet A, Wyatt J. Thresh-olds for activation of rabbit retinal ganglion cells with an ultrafine, extra-cellular microelectrode. Invest. Ophthalmol. Vis. Sci. 2003; 44:3533–3543. [PubMed: 12882804]

[20]. Weiland JD, Humayun MS, Dagnelie G, de Juan E Jr. Greenberg RJ, Iliff NT. Understanding the origin of visual percepts elicited by electrical stimulation of the human retina. Graefes Arch. Clin. Exp. Ophthalmol. 1999; 237:1007–1013. [PubMed: 10654170]

[21]. Humayun M, Propst R, de Juan E Jr. McCormick K, Hicking-botham D. Bipolar surface electrical stimulation of the vertebrate retina. Arch. Ophthalmol. 1994; 112:110–116. [PubMed: 8285877]

[22]. Doty RW, Grimm FR. Cortical responses to local electrical stimulation of retina. Exp. Neurol. 1962; 5:319–334. [PubMed: 13887504]

[23]. Dowson WW, Radke ND. The electrical stimulation of the retina by indwelling electrodes. Invest. Ophthalmol. Vis. Sci. 1977; 16:249–252. [PubMed: 844981]

[24]. Margalit E, Thoreson WB. Inner retinal mechanisms engaged by retinal electrical stimulation. Invest. Ophthalmol. Vis. Sci. 2006; 47:2606–2612. [PubMed: 16723477]

[25]. Fried SI, Hsueh HA, Werblin FS. A method for generating precise temporal patterns of retinal spiking using prosthetic stimulation. J. Neurophysiol. 2006; 95:970–978. [PubMed: 16236780]

[26]. Stett A, Barth W, Weiss S, Haemmerle H, Zrenner E. Electrical multisite stimulation of the isolated chicken retina. Vis. Res. 2000; 40:1785–1795. [PubMed: 10814763]

[27]. Sekirnjak C, Hottowy P, Sher A, Dabrowski W, Litke AM, Chichilnisky EJ. Electrical stimulation of mammalian retinal ganglion cells with multielectrode arrays. J. Neurophysiol. 2006; 95:3311–3327. [PubMed: 16436479]

[28]. Grumet AE, Wyatt JL Jr. Rizzo JF III. Multi-electrode stimulation and recording in the isolated retina. J. Neurosci. Methods. 2000; 101:31–42. [PubMed: 10967359]

[29]. Zrenner E, Stett A, Weiss S, Aramant RB, Guenther E, Kohler K, Miliczek KD, Seiler MJ, Haemmerle H. Can subretinal microphotodiodes successfully replace degenerated photoreceptors? Vis. Res. 1999; 39:2555–2567. [PubMed: 10396624]

[30]. Greenberg, R. Ph.D. dissertation, Dept. Biomed. Eng., Johns Hopkins Univ. Baltimore, MD: 1998. Analysis of electrical stimulation of the vertbrate retina— Work towards a retinal prosthesis.

[31]. Segev R, Goodhouse J, Puchalla J, Berry MJ. Recording spikes from a large fraction of the ganlion cells in a retinal patch. Nat. Neurosci. 2004; 7:1154–1161. [PubMed: 15452581]

[32]. Werblin FS. Transmission along and between rods in the tiger salamander retina. J. Physiol. 1978; 280:449–470. [PubMed: 211229]

[33]. Segev R, Puchalla J, Berry MJ. Functional organization of ganglion cells in the salamander retina. J. Neurophysiol. 2006; 95:2277–2292. [PubMed: 16306176]

[34]. Ahuja, A.; Nasiatka, P.; Song, D.; Berger, TW.; Tanguay, A. A biomimetic electronic prosthetic for hippocampus: Planar conformal multielectrode arrays for VLSI/hippocampal slice interface; presented at the Soc. Neurosci.; San Diego, CA. 2004;

[35]. Gholmieh G, Soussou W, Han M, Ahuja A, Hsiao MC, Song D, Tanguay AR Jr. Berger TW. Custom-designed high-density conformal planar multielectrode arrays for brain slice electrophysiology. J. Neurosci. Methods. 2006; 152:116–129. [PubMed: 16289315]

[36]. Whalen JJ, Weiland JD, Searson PC. Electrochemical deposition of platinum from aqueous ammonium hexachloroplatinate solution. J. Electrochem. 2005; 152:C738–C743.

[37]. Hung, A.; Zhou, D.; Greenberg, R.; Judy, JW. Micromachined electrodes for retinal prostheses; presented at the EMBS; Houston, TX. 2002;

[38]. Johnson AM, Sadoway DR, Cima MJ, Langer R. Design and testing of an impedance-based sensor for monitoring drug-delivery. J. Electrochem. Soc. 2005; 152:H6–H11.

[39]. Jensen RJ, Ziv OR, Rizzo JF III. Thresholds for activation of rabbit retinal ganglion cells with relatively large, extracellular microelectrodes. Invest. Ophthalmol. Vis. Sci. 2005; 46:1486–1496. [PubMed: 15790920]

[40]. Ranck JB Jr. Which elements are excited in electrical stimulation of mammalian central nervous system: A review. Brain Res. 1975; 98:417–440. [PubMed: 1102064]

[41]. Cole KS. Electric conductance of biological systems. Proc. Cold Spring Harbor Symp. Quant. Biol. 1933:107–116.

[42]. Gouras P. Identification of cone mechanisms in monkey ganglion cells. J. Physiol. 1968; 199:533–547. [PubMed: 4974745]

[43]. Crapper DR, Noell WK. Retinal excitation and inhibition from direct electrical stimulation. J. Neurophysiol. 1963; 26:924–947. [PubMed: 14084167]

[44]. Shimazu K, Miyake Y, Watanabe S. Retinal ganglion cell response properties in the transcorneal electrically evoked response of the visual system. Vis. Res. 1999; 39:2251–2260. [PubMed: 10343806]

[45]. Varela C, Igartua I, de La Rosa EJ, de La Villa P. Functional modifications in rod bipolar cells in a mouse model of retinitis pigmentosa. Vis. Res. 2003; 43:879–885. [PubMed: 12668057]

[46]. Ziv OR, Rizzo JF, Jensen RJ. *In vitro* activation of retinal cells: Estimating location of stimulated cell by using a mathematical model. J. Neural. Eng. 2005; 2:S5–S15. [PubMed: 15876655]

[47]. Grill WM Jr. Mortimer JT. The effect of stimulus pulse duration on selectivity of neural stimulation. IEEE. Trans. Biomed. Eng. Feb; 1996 43(2):161–166. [PubMed: 8682527]

[48]. Rizzone M, Lanotte M, Bergamasco B, Tavella A, Torre E, Faccani G, Melcarne A, Lopiano L. Deep brain stimulation of the subthalamic nucleus in Parkinson's disease: Effects of variation in stimulation parameters. J. Neurol. Neurosurg. Psychiatry. 2001; 71:215–219. [PubMed: 11459896]

[49]. Kwon BJ, van den Honert C. Dual-electrode pitch discrimination with sequential interleaved stimulation by cochlear implant users. J. Acoust. Soc. Amer. 2006; 120:EL1–EL6. [PubMed: 16875252]

[50]. Lawson DT, Wilson BS, Finley CC. New processing strategies for multichannel cochlear prostheses. Prog. Brain Res. 1993; 97:313–321. [PubMed: 8234758]

[51]. White MW, Merzenich MM, Gardi JN. Multichannel cochlear implants: Channel interactions and processor design. Arch. Otolaryngol. 1984; 110:493–501. [PubMed: 6547597]

[52]. O'Brien BJ, Isayama T, Richardson R, Berson DM. Intrinsic physiological properties of cat retinal ganglion cells. J. Physiol. 2002; 538:787–802. [PubMed: 11826165]

[53]. Rubinstein JT, Spelman FA, Soma M, Susserman MF. Current density profiles of surface mounted and recessed electrodes for neural prostheses. IEEE Trans. Biomed. Eng. Nov; 1987 34(11):864–875. [PubMed: 3319885]

[54]. Wagner C. Theoretical analysis of the current distribution under circular dispersive electrodes. J. Electrochem. Soc. 1951; 98:116–119.

[55]. Forster, RJ. Microelectrodes—Retrospect and prospect. In: Bard, AJ.; Stratman, M., editors. Electroanalytical Methods. Wiley; New York: 2005.

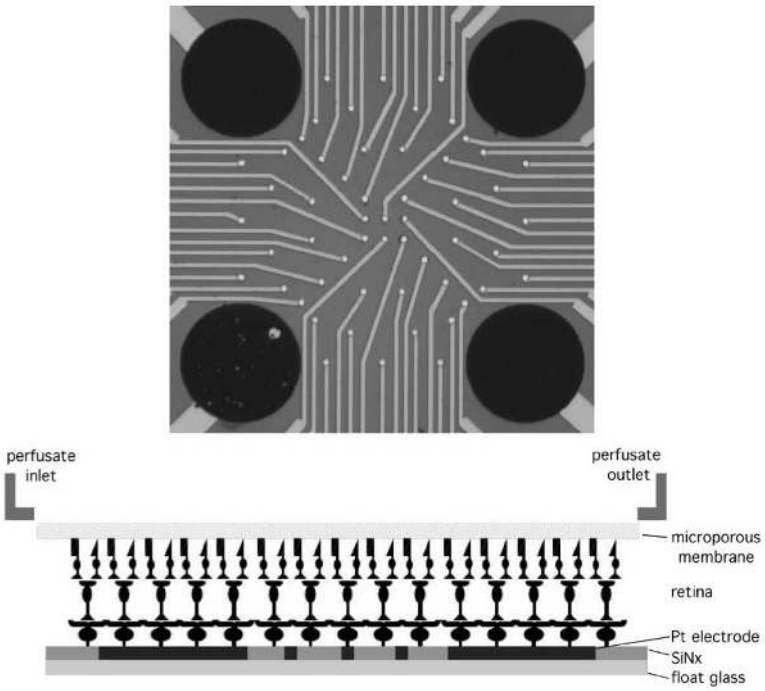

Fig. 1.

Photomicrograph of custom retinal multielectrode array with 200-μm-diameter stimulating Pt-electroplated electrodes and 10-μm-diameter electronbeam evaporated Pt thin-film recording electrodes (top). While the larger stimulating electrodes are electroplated to increase effective surface-area for charge injection, the smaller electrodes are not so as to keep the impedance high enough to record only single unit activity and adequately localize ganglion cell body position. Schematic of retina, gently pressed ganglion cell side down on custom MEA with microporous dialysis membrane (bottom).

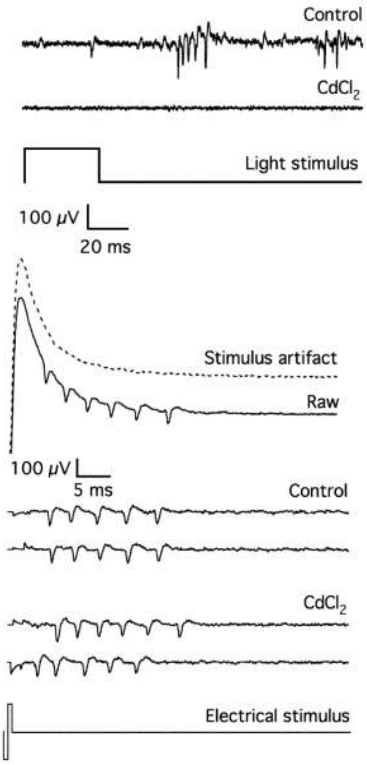

Fig. 2.

ON and OFF light response of a cell to a 40 ms full-field shutter flash before (control) and after $CdCl_2$ application (top). Proof-of-concept of artifact subtraction method to reveal tonic ganglion cell response corrupted by stimulus artifact (middle). Direct ganglion cell excitation is confirmed by noting persistence of recorded spikes before (control) and after $CdCl_2$ application. Schematics of the light and electrical stimuli are shown to give a time reference (*raw* is before subtraction and *control* is after subtraction) (bottom).

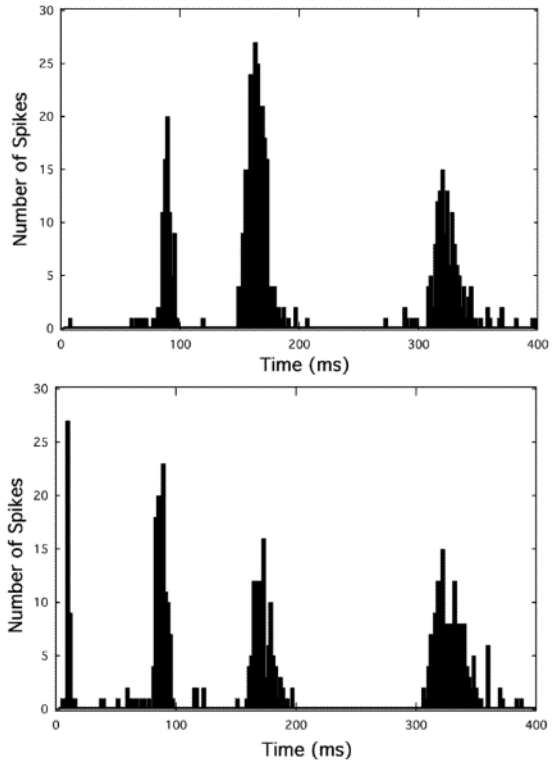

Fig. 3.
PSTH for two ganglion cells representative of reverberating response to stimulation (50 pulse train of 400 μs cathodic-first biphasic pulses). These responses were blocked by both the APV/CNQX/PDA cocktail and $CdCl_2$ in concentrations described in Section II.

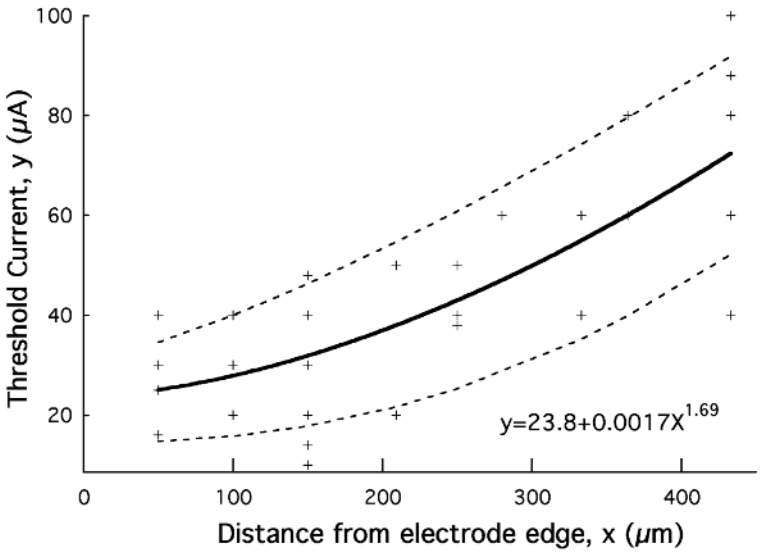

Fig. 4.

Threshold current versus distance from the edge of a 200-μm-diameter stimulating electrode for presynaptic excitation ($n = 42$ cells). Power function best-fit curve of data (solid line) and 95% confidence interval (dotted lines) are shown. Greater variability is observed at sites further from the edge of the stimulating electrode due to excitation of the nonlinear retinal network. All responses were blocked by both the APV/CNQX/PDA cocktail and $CdCl_2$ in concentrations described in Section II.

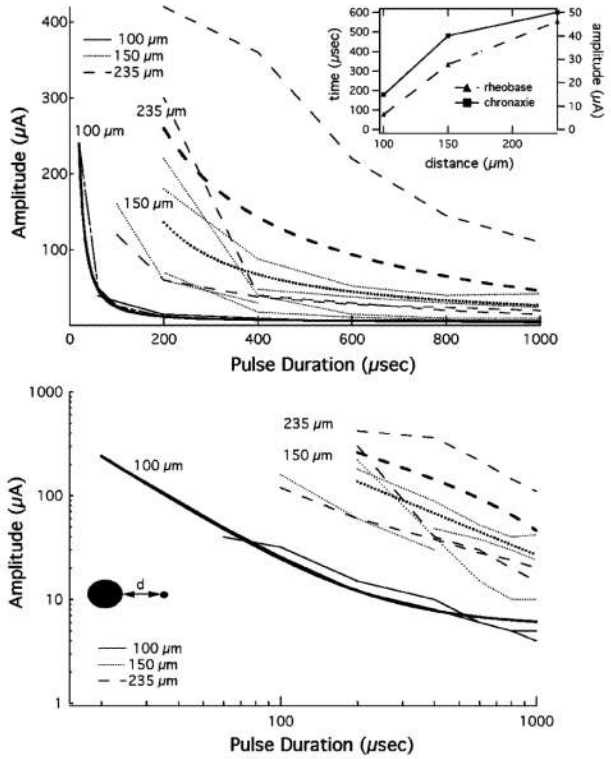

Fig. 5.

Strength-duration data for cells at different distances [100 ($n = 2$), 150 ($n = 4$), and 235 μm ($n = 3$)] from the edge of a 200-μm-diameter electrode (top). Best-fit curves of mean data at each distance are plotted using the corresponding bold trace pattern of the data taken from individual cells. The greater current amplitude spacing between average chronaxie curves at 200 μs versus 1 ms suggests method of using short pulses to best code for brightness while not increasing exciation area. (Inset) Chronaxie and rheobase values, plotted on time (in microseconds) and current amplitude (in microamperes) versus distance from stimulating electrode edge (in micrometers) axes, respectively. Log-log plot of strength-duration data. All responses were blocked by both the APV/CNQX/PDA cocktail and $CdCl_2$ in concentrations described in Section II (bottom).

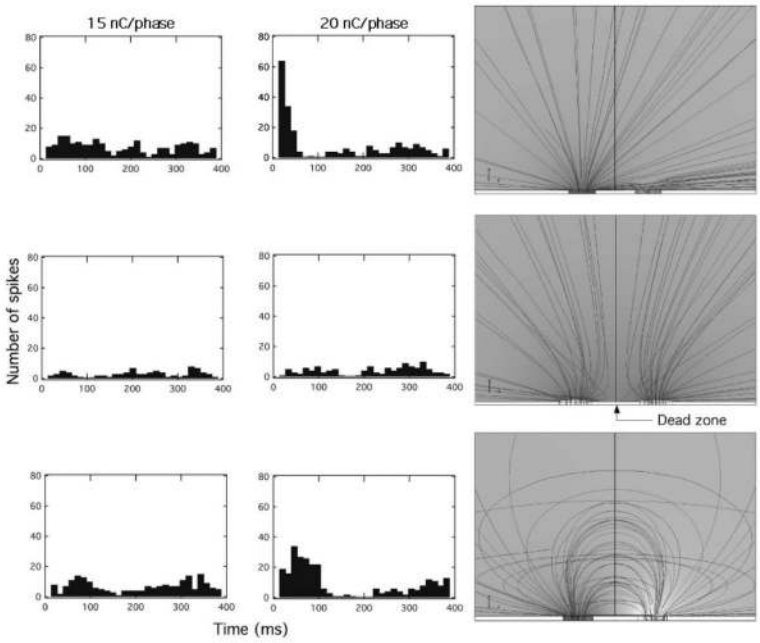

Fig. 6.

PSTHs of subthreshold (15 nC/phase) (left column) and suprathreshold (20 nC/phase) (middle column) stimulation for monopolar (top row), dual monopolar with adjacent stimulating pads in parallel (second row), and bipolar stimulation (third row). A suprathreshold response is observed in the 20 nC/phase monopolar case; the low firing rates in all six cases are due to spontaneous firing. Electrostatic finite-element modeling results showing the direction of the gradient of the electric field for monopolar (top; right column), dual monopolar (middle), and bipolar stimulation using neighboring stimulating electrodes (bottom).

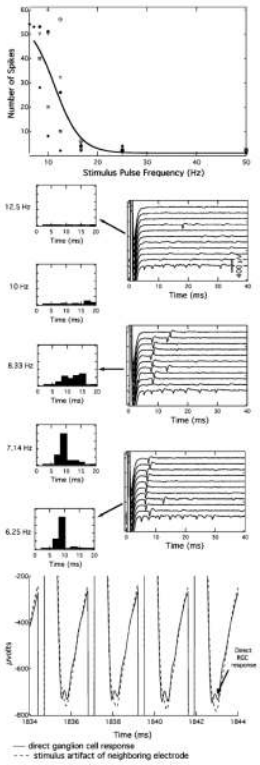

Fig. 7.

Number of presynaptic spikes elicited in a 50 pulse stimulus train versus pulse frequency using 400 μs cathodic first biphasic pulses ($n = 6$) (top). Representative histograms (left) and raw data (right) of suppression of presynaptically driven responses above 10 Hz for a single cell (middle). The raw data (right) depicts responses to successive pulses at pulse frequencies of (from bottom to top) 6.25, 8.33, and 12.5 Hz. The first pulse of the train is at the bottom of the graph. Recorded stimulus artifact with a direct ganglion cell response (solid line) at a stimulation frequency of 500 Hz, ascertained by the application of $CdCl_2$, and recorded stimulus artifact without a ganglion cell response (dashed line; bottom). These two recording electrodes were equidistant from the stimulating site; the difference in the two shows a repeatable ganglion cell response even at 500 Hz (marked with an arrow). This direct ganglion cell excitation is above the frequency at which presynaptic excitation is suppressed.